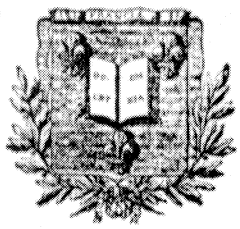

COLLÈGE DE FRANCE
Laboratoire de Physique Corpusculaire

LPC 93 34

GAMMA RAY SPECTRUM OF THE CRAB NEBULA IN THE MULTI TeV REGION

P. Baillon
CERN, Geneva, Switzerland

L. Behr, S. Danagoulian, B. Dudelzak, P. Eschtruth, R. Riskalla, P. Roy
LAL, Université Paris Sud, Orsay

A. Djannati-Ataï, P. Espigat, C. Ghesquière, P. Schune
Collège de France, IN2P3 - CNRS

B. Fabre, C. Meynadier
Université de Perpignan

G. Fontaine, J. Vrana
LPNHE X, Ecole Polytechnique, Palaiseau

R. George, F. Kovacs, Y. Pons, M. Rivoal, T. Socroun, A.M. Touchard
LPNHE, Université Paris 6 - 7

COLLEGE DE FRANCE, IN2P3-CNRS, Laboratoire de Physique Corpusculaire,
11 Place Marcelin Berthelot, F-75231 Paris Cedex 05, FRANCE

Submitted to Astro-Particle Physics

Gamma ray spectrum of the Crab nebula in the multi TeV region

THEMISTOCLE Collaboration

P. Baillon [2], L. Behr [3], S. Danagoulian [3,*], A. Djannati-Ataï [1], B. Dudelzak [3], P. Espigat [1], P. Eschstruth [3], B. Fabre [6], G. Fontaine [5], R. George [4], C. Ghesquière [1], F. Kovacs [4], C. Meynadier [6], Y. Pons [4], R. Riskalla [3], M. Rivoal [4], P. Roy [3], P. Schune [1,**], T. Socroun [4], A.M. Touchard [4], J. Vrana [5].

[1] Collège de France 11 Pl. M. Berthelot F-75231 Paris Cedex 05

[2] CERN CH-1211 Geneva 23

[3] LAL Bat.200 Univ. Paris Sud F-91405 Orsay

[4] LPNHE Univ. Paris 6-7 Tour 33 R.d.C. 4 Pl.Jussieu F-75252 Paris Cedex 05

[5] LPNHE X Ecole Polytechnique F-91128 Palaiseau

[6] Univ. de Perpignan Ave de Villeneuve F 66025 Perpignan Cedex

[*] Permanent adress: Yerevan Ph. Inst. Alikhanian Br. St. 2 Yerevan 375036 Armenia

[**] Now at DAPNIA CEN Saclay F-91191 Gif s. Yvette Cedex

Abstract

The THEMISTOCLE array of 18 Cerenkov detectors which has a 3 TeV gamma energy threshold, has detected a signal from the Crab nebula at a 5.8 standard deviation level. Information on the energy spectrum is obtained in the range 3 to 15 TeV . The integrated flux can be fitted with the form :

$$\Phi(>E)= (3.7 \pm 0.5)\ 10^{-12}\ (E / 5)^{-1.5 \pm 0.20}\ cm^{-2}\ s^{-1} \qquad (E \text{ in TeV})$$

compatible with the extrapolation of results at lower energies.

The Crab signal is used to measure the angular resolution of the multi-telescope technique. The value obtained is 2.3 mr (0.15°) in agreement with the results of simulations, and confirms the interest of this new method for multi-TeV gamma-ray detection.

Keywords: Astrophysics, gamma astronomy, telescope counters, Crab nebula

1 Introduction.

The THEMISTOCLE experiment is located near Targasonne in the French Pyrenees, at lat. 42.50° N, lon. 1.97° E and mean altitude 1650m. Its original motivation was to test the method of time sampling on the Cerenkov wave front in order to obtain milliradian accuracy in the reconstruction of the direction of the primary photon in the multi-TeV energy range. From flux and spectrum measurements around 1 TeV [1], it was reasonable to hope for a detectable flux from the Crab nebula at higher energies.

Our observations of the Crab reported herein, were concentrated in two winter periods, 1990-1991 and 1991-1992, totalizing 162 hours of on-source and 204 h of off-source data taking. We report here on the results of these observations leading to a clear signal and a measurement of the energy spectrum. In the analysis, event selection is mostly based on angular resolution criteria with some hadronic rejection.

2 Principle of the Experiment.

The experiment was defined on the basis of a detailed Monte-Carlo simulation of both gamma and hadron showers in atmosphere [2], in order to study the characteristics of the method and to optimize the choice of the parameters.

It was shown [3] that the wave front of the Cerenkov light emitted during the propagation of the shower in the atmosphere has the form of a very flat cone with a lateral extension of the order of 200 meters. The average value of the angle characterizing the cone is 15 mr. It is not sensitive to energy in our range.

The profile of the Cerenkov photon arrival time along the propagation direction at the detector altitude corresponds to a steep 1 ns rise time and a 2 ns mean width. This sharp signal leads to the possibility of an accurate measurement of the instant of the wave front arrival at the detector.

The conical form of the wave front can be reconstructed, providing both the direction of the primary photon and the ground impact point of the shower axis. The angular resolution obtained depends principally on the spacing between detectors, on their number and on the precision of the individual timing measurements [4].

The total number of Cerenkov photons hitting the ground is, on the average, proportional to the energy of the primary particle, but due to the limited extension of the field, only part of the image is sampled by a variable number of telescopes. A method described later, based on the radial distribution of the density of Cerenkov light, has been applied to reconstruct the energy.

3 Experimental Set-up.

The experiment consists of 18 Cerenkov telescopes distributed over a roughly elliptical field of major and minor axes 280 and 190 m respectively. The positions of the detectors are shown in Fig 1. Each telescope has a 800 mm diameter parabolic mirror with a single fast photomultiplier tube (RTC XP2020) at its focus. We have used the mirror mountings of the THEMIS solar power installation which stopped operating in 1986. Each has two microprocessor-controlled DC motors and provides a 2 mr pointing accuracy. This is adequate to avoid excessive loss of photons, which, due to pointing error, could fall outside the 40 mr diameter optical aperture used for this analysis. The optical axis of each telescope is directed towards the calculated position of the source being observed.

The phototube signal, after a 10x voltage gain amplifier with two outputs, is sent locally to a constant-fraction discriminator to generate a timing signal, and via cable to a centrally located ADC . The timing signals are sent to the TDC's (0.1 ns least count, full range 600 ns), and the trigger system, also centrally located.

The relative timing calibration combined with verification of the photo-multiplier tube gains, done in general twice each night, use a pulsed nitrogen laser emitting from a point at the 70 meter level of the THEMIS solar plant tower overlooking the field [5]. The data from the appropriate calibration runs are used to correct the timing measurements for a shower data run. Drifts and systematic variations can be corrected for on the 50 ps level.

Measurements using the laser also provide the timing uncertainty as a function of the number of photo-electrons through the relation

$$\sigma_t = \left(a^2 + \frac{b^2}{N_{Phe}} \right)^{\frac{1}{2}} \qquad (1)$$

where :

σ_t is expressed in ns

N_{Phe} is the number of photo-electrons.

a and b vary from PM to PM with typical values of 0.17 and 2.7 ns respectively.

To keep down the singles rates induced by the night sky background, we have used a discriminator threshold at about 4 sd of this background fluctuation.

Each telescope contributes to a majority logic coincidence trigger through computer controlled variable delay lines. The maximum delay range (512 ns) limits the zenit angle for acquisition to about 35 . The average trigger rate is 0.16 events/sec for a minimum of 10 telescopes hit and 0.09 events/sec for a minimum of 12 .

Accidental triggers due to lower energy showers in coincidence with single counts occur at an estimated level lower than 10^{-2}.

4 Monte-Carlo Simulations.

The Monte-Carlo program is based on work done for the CERN-DELPHI experiment [2]. It generates without analytical approximation gamma ray and proton showers in the atmosphere, following charged particles and gammas, without weighting, down to an energy of 100 MeV, and following their Cerenkov emission down to the ground [3]. The effect of the earth's magnetic field is taken into account.

The optics and electronics distort deeply the primitive Cerenkov pulses: the fast 1 ns rise time mentionned earlier becomes more like 3 ns, and the 2 ns mean pulse width increases to 5 ns. In order to have realistic simulation of the detector response (time and amplitude) in the Monte-Carlo the detector is simulated in detail, including mirror aberrations and PM , amplifier and CFD responses. This detailed treatment is necessary to evaluate precisely the acceptance of the apparatus.

Only two parameters are left free to be adjusted via the experimental data. One is a global scaling factor (R) on the number of Cerenkov photons. It is connected to the fact that the standard atmosphere absorption used in the program has to be adjusted to the specific experimental conditions. The other free parameter is connected to the total gain of the electronic chain (G).

The shapes of the experimental distributions reproduced by the simulation (ADC values, triggering PM multiplicity) are very sensitive to G but depend weakly on R. They are used to adjust the G parameter. On the other hand, the trigger rate depends essentially on the value of R and is used to adjust it. The comparison between the experimental and simulated distributions, after parameter adjustment is shown in Figs 2 and 3.

The atmospheric absorption may change from day to day and even on shorter time scales, inducing trigger rate variations and changes in R values. In our data analysis we have corrected for the main fluctuations of the trigger rate. Nevertheless the bulk of the systematic errors in the energy measurement is due to the uncertainty on R, coming both from the simulation and the measurement of the trigger rate.

5 Analysis Method

5.1 Cone reconstruction

Event reconstruction involves fitting the six parameters which characterize the cone : the three coordinates of the cone's apex, the axis direction and the angle by which the cone departs from flatness.

A non linear fitting procedure minimizes the $\chi 2$ obtained from the difference between measured times and expected times for the cone, normalized to the estimated

errors. A minimum of 12 points ensures a 6 constraint fit and is necessary to obtain good accuracy both in direction and in position of the cone apex [3].

The timing errors, σ_t, are derived from the amplitudes according to the formula (1) . Fig 4 shows the time residuals for the fitted events with a $\chi 2$ probability > 0.10 . The mean value is 0.33 ns.

The deviation of the reconstructed shower direction from the pointing direction is expressed by two Euler angles, u_R and u_D defined in a local coordinate system whose axis are parallel to the local Right Ascension and Declination, respectively. The angles u_{Ro} and u_{Do} give the deviation of the Crab peak signal from the Crab pulsar direction (RA 83.477°, Dec 22.011° for Jan. 1st, 1990).

The angular acceptance, in u_R and u_D, of the apparatus is well represented for the events selected within the cuts which will be described later, at least up to 25 mr, by a two dimensional gaussian of 11 mr standard deviation , with tails extending up to 50 mr. A signal from a point like source should appear as a sharp gaussian peak superimposed on the 11 mr wide acceptance curve for hadrons.

5.2 Energy measurement and hadronicity.

The individual energy of each event is obtained by comparing the ADC values converted into photo-electrons, to the equivalent average radial density distributions obtained by Monte-Carlo generation of gamma showers, at the reconstructed radial distances from the apex. These radial distributions have been generated at five energies : 1, 3, 10, 30 and 100 TeV.

Fitting the log of the radial density, a smooth function of energy and radius is obtained by polynomial interpolation, (Fig. 5), to which the experimental measurements are fitted by minimizing $\chi 2$ in energy. From Monte-Carlo studies it has been determined that the energy estimate is improved by using only those telescopes lying between 20 and 130 m from the apex. At smaller distances the uncertainty on the apex reconstruction degrades the prediction in a region where the variations are rapid, while at large distance the density is too weak to provide useful information.

The individual measurement errors used in the fit are given by the square root of the number of photo-electrons from the interpolated reference curves.

The process of energy fitting proceeds in two stages a and b:

a) The radial distribution is fitted to the measurements and a first value of the energy and the normalized $\chi 2$ is obtained. This value of $\chi 2$ is representative of the large variations in Cerenkov light intensity which may occur in the case of a hadron shower, much less regular than a gamma shower. We call this $\chi 2$ statistic: the" hadronicity". Its distribution is shown in Fig. 6 .

b).We eliminate in two successive steps the measurements having the largest partial $\chi 2$. If the fit converges after removal of these two measurements we then obtain an estimation of the energy and its error.

The error on the fitted energy is deduced from the mean value of the dispersion of the experimental points around the fitted curve. The comparison between the distribution of estimated error for hadronic Monte-Carlo events: Fig 7 a, and for real hadronic events: Fig 7 b, shows that the error is correctly estimated for hadrons, taking into account that the ratio of low energy to high energy reconstructed events is higher in Monte Carlo than in real events. We then conclude that our estimation for gammas is valid. For gammas the average relative error on energy , $<\Delta E/E>$, ranges from 20% at 3 TeV to 15% at 20 TeV.

The absolute energy calibration depends strongly on the trigger rate. To account for that, when dealing with energy, we select runs (typically 3 hours in duration) where the event rate exceeded a threshold of 0.06 events/sec, for an average value of 0.09 evts/sec, and correct the energy according to their deviation from the average. The cut at 0.06 eliminates those runs where the correction would be too large.

The absolute energy threshold for gamma rays is 3 TeV, whereas for hadrons, which in our experimental conditions produce an average of 30% less Cerenkov light than a gamma of the same energy, the threshold is accordingly close to 4 TeV. Moreover on the high energy side the limited range of our ADC's and saturations elsewhere decrease our ability to treat events beyond 20 TeV for all particles.

6 Crab Signal

We observed the Crab nebula during two consecutive periods: 67 hours from October 1990 to February 1991, and 95 hours from January 1992 to March 1992, which represent respectively 31362 and 45164 registered events. For the analysis we used a similar sample of 56792 off-source events. These off-source events are obtained during the same nights as the on-source data and at the same declination but with a delayed right ascension, in order to approach as much as possible the on-source conditions without losing on-source data taking time.

Within statistical variations the data taken one year apart agree and after being checked for consistency have been added together for a global result.

Cuts are applied to reject badly reconstructed events. They require:

1) A minimum of 12 telescopes retained by the cone fitting procedure.

2) Cone angle between 10 and 20 mr.

3) Cone apex within an ellipse having axes of 200 and 190 m, centered on the field.

4) $\chi 2$ probability > 0.30

5) Shower direction less than 15 mr from the source direction.

The selected sample then corresponds to 6516 on-source and 5647 off-source events.

We have checked that our reconstruction method, applied to the Monte Carlo events is correct, by histogramming the difference between initial and reconstructed parameters : the direction (u_R, u_D) and the cone apex (X, Y). The variance σ (D) of these distributions are reported in Table 1 for hadrons and photons. Moreover in this table we show the comparison of the errors σ (C) obtained from the covariance matrix of the fit for the real and Monte Carlo events.

A maximum likelihood method described in Annex 1, is applied to test for the existence of a source signal against the hypothesis of a null signal. The four parameters left free in the adjustment are :

1) The width σ of the two-dimensional signal assumed to have a gaussian distribution (39% of the signal is contained within one σ)

2) The angles u_{Ro}, u_{Do} giving the deviation of the signal peak from the source direction.

3) The ratio S/B of the amplitudes of the signal to the background at the peak position.

The results are summarized in Table 2.

We may remark that the fitted source direction is in agreement with the pulsar direction and the uncertainty on the direction of the source corresponds to 1.5 arc minute.

The signal to background level at the peak position is S/B = 0.58±0.10 without any hadronicity rejection.

The resulting signal is shown in Fig 8 as a background-subtracted two dimensional plot with axes u_R, u_D, centered on u_{Ro} and u_{Do} , and in Fig 9, where the events are given as a function of γ^2, γ being the angle of the reconstructed cone axis relative to the signal position centered on u_{Ro}, u_{Do} .

7 Energy Spectrum

We have estimated the integral flux starting from our threshold of 3 TeV and proceeding by steps of 2 TeV, up to 15 TeV. Beyond that value the statistics are too scarce to give a reliable result.

In order to be in the best conditions to evaluate the energy we applied the cut on a minimum trigger rate explained in § 5. This cut reduces the data sample by 21%.

To get a better signal to background ratio we have rejected the events where the hadronicity defined earlier is > 3.5. This cut eliminates less than 1% of the gammas and is particularly efficient for rejecting hadrons over 10 TeV.

The value of the signal for the different energy thresholds is obtained by the same maximum likelihood method as used before. The results are shown in Table 3. The

significance of the signal weakens as the energy increases becoming marginal beyond 15 TeV.

The flux is then evaluated through the formula :

$$\Phi(>E) = \frac{N(>E)}{S \times T_{tot} \times \varepsilon(>E)}$$

N(>E): the number of gammas over the threshold energy E.

S: the useful area : πx100x95 10^4 = 2.98 10^8 cm^2 .

T_{tot} : the total useful time = 453829 s .

$\varepsilon_{(>E)}$: the acceptance calculated by Monte-Carlo.

To evaluate the acceptance $\varepsilon_{(>E)}$ we generated gamma events according to a differential spectrum in $E^{-2.4}$, processed all events through the simulated detector, the reconstruction program and the energy evaluation and finally applied the same final cuts.

The acceptance is then obtained, over a given energy threshold, as the ratio of accepted events to initial events and shown in Table 3.

The final results on the fluxes are also shown in Table 3 and plotted in Fig 10 .

We use an average spectral index to fit over all our points, although the hypothesis of a constant value of this index, compatible with our data, may not be justified in this range of energy. Gamma production through an inverse Compton scattering process [6] would lead to a smoothly varying index. Moreover to minimize the effect of correlation between measurements, the spectrum has been fitted using only the points at 3, 9 and 15 TeV, to the formula:

$$\Phi(>E) = (3.7 \pm 0.5)\ 10^{-12}\ (E / 5)^{-1.5 \pm 0.20}\ cm^{-2}\ s^{-1} \qquad (E \text{ in TeV})$$

Results from other experiments [7], are also indicated in Fig. 10, as well as the extrapolation of the results of [1a] obtained for the energy range between 0.4 and 4. TeV

** Foot-note

The most recent results about the Crab spectrum reported at the last ICRC at Calgary (19-30 July 1993) are not implemented on the graph, Fig. 10.

8 Conclusions.

A gamma signal of energy greater than 3 TeV from the Crab Nebula has been detected with a 5.8 standard deviation significance level in an analysis based only on angular resolution. The significance is increased to 6.5 standard deviation while selecting events over a 3 TeV cut.

We have demonstrated the ability of the time sampling method on the Cerenkov wave front to provide good angular resolution : 2.44 ±0.30 mr, slightly higher than the results of our simulation.

The error on the source direction is found to have systematics less than 0.5 mr (1.7 ') providing the possibility of identifying sources with a high degree of precision.

In spite of the limited number of sampling points, it was possible to obtain an accurate energy measurement estimated by Monte-Carlo to be at the 15-20 % level, but the systematics on the energy may still be of the order of 20%.

The evidence for a signal does not explicitly rely on hadron rejection based on different shower properties. Nevertheless the trigger itself and many cuts applied during event processing, both in reconstruction and in energy evaluation, do in fact reject preferentially hadrons and hadron-like showers. If we estimate the efficiency of the overall background rejection as the ratio between the expected number of hadrons under our gamma peak (25 mr^2) and those observed at the equivalent gamma energy, this rejection varies with energy threshold from roughly a factor of 20 near 3 TeV to 5 beyond 15 TeV, while preserving 80% of the gammas.

The gamma ray spectrum from the Crab has been shown to extend up to 15 TeV without a fast drop. It is not possible at the present time to draw any conclusions about the region above 15 TeV due to statistical limitations.

Only part of this data was obtained with a precise clocking, thus preventing us to look efficiently for a pulsed signal phased to the pulsar period. Our next data will allow this research.

Acknowledgments.

We wish to thank E.D.F. (Electricité de France) for granting us use of the facilities of the THEMIS site without charge. The experiment was funded by the I N2 P3 (Institut National de Physique Nucléaire et de Physique des Particules) of the CNRS, France.

Annex 1 : Likelihood method and significance of the signal.

Let $\vec{u} = \{ u_R, u_D \}$ be the measured shower direction. In the hypothesis of a Gaussian form for the signal, the probability distribution function (p.d.f.) of $\vec{u}$ is

$$P_s(\vec{u}) = \frac{A(\vec{u}) \left[1 + (\frac{S}{B}) \exp - \frac{(\vec{u} - \vec{u}_0)^2}{2\sigma^2} \right]}{\int d\vec{u}\, A(\vec{u}) \left[1 + (\frac{S}{B})\, \rho \right]}$$

$$\text{where} \quad \rho = \frac{\int d\vec{u}\, A(\vec{u}) \exp - \frac{(\vec{u} - \vec{u}_0)^2}{2\sigma^2}}{\int d\vec{u}\, A(\vec{u})}$$

The four parameters $(\frac{S}{B})$, $\vec{u_o}$ and σ are defined in the text.

We will use $\bar{\theta}$ to designate this set of four parameters.

$A(\vec{u})$ is the angular acceptance of the detector.

In the hypothesis of a null signal (H_o) the p. d. f. is

$$P_o(\vec{u}) = \frac{A(\vec{u})}{\int d\vec{u}\, A(\vec{u})}$$

The following statistic, which makes use of the ratio *Ls/Lo* of the likelihoods with and without signal,

$$T = 2 \log Ls/Lo = 2 \left\{ \underset{\theta}{\text{Max}} \sum_{i=1}^{N_{ON}} \log P_s(\vec{u_i}) - \sum_{i=1}^{N_{ON}} \log P_o(\vec{u_i}) \right\}$$

- provides a parametric estimate for $\bar{\theta}$, the set of four parameters
- is a statistic whose distribution in the hypothesis H_o follows a χ^2 law with four degrees of freedom.

In the followind N_{ON} and N_{OFF} are the numbers of on-source and off-source events, respectively.

After simplification one obtains

$$T = 2 \sum_{i=1}^{N_{ON}} \log \left(1 + (\frac{S}{B}) \exp - \frac{(\vec{u_i} - \vec{u_o})^2}{2\sigma^2} \right) - 2 N_{ON} \log \left(1 + (\frac{S}{B})\rho \right).$$

We note that the values $A(\vec{u_i})$ disappear as is the case with any maximum likelihood estimate.

At this point this analysis becomes more specific to our experiment, since the only information we have about ρ is provided by the off-source data. The sum over the off-source events converges towards ρ if the acceptance is the same for the on-source and the off-source events.

$$\hat{\rho} = \frac{1}{N_{OFF}} \sum_{j=1}^{N_{OFF}} \exp - \frac{(\vec{u_j} - \vec{u_o})^2}{2\sigma^2}$$

The fact that ρ is not known with infinite precision but estimated by $\hat{\rho}$ implies that to first order in $\hat{\rho} - \rho$, the estimate of T for the value $\hat{\rho}$ is

$$T(\hat{\rho}) = T(\rho) - \frac{2\, N_{ON}\, (\frac{\hat{S}}{B})\, \sigma_\rho\, y}{1 + \rho\, (\frac{\hat{S}}{B})}$$

where σ_ρ is the standard deviation of the statistic $\hat{\rho}$ and y a normal variable.

$T(\rho)$ is a bilinear form of the four estimates, terms including $(\frac{\hat{S}}{B})$ being correlated to the additional one.

A study of the bilinear form for $\frac{S}{B} \to 0$ (hypothesis H_0) shows that the correlation between $\frac{\hat{S}}{B}$ and the three other parameters is quite small. Consequently,

$$T(\hat{\rho}) \approx \chi^2_{(3)} + x^2 + \alpha\ x\ y$$

where

$x = \frac{\hat{S}/S}{\sigma_{S/B}}$ is a normal variable and

$$\alpha = -\frac{2\, N_{ON}\, \sigma_{S/B}\, \sigma_\rho}{1 + \rho\, (\frac{\hat{S}}{B})}$$

Furthermore, for $S = 0\ (H_0)$, $\sigma_{\hat{S}/B}\, \sigma_{\hat{\rho}} = \frac{1}{\sqrt{N_{ON}\, N_{OFF}}}$ giving $\alpha = -\frac{-2\sqrt{\frac{N_{ON}}{N_{OFF}}}}{1 + \rho\, (\frac{\hat{S}}{B})}$?

The random variable $z = x^2 + \alpha\ x\ y$ follows the law

$$\frac{1}{\pi|\alpha|}\, e^{z/\alpha^2}\, K_0\, (\left|\frac{\sqrt{1+\alpha^2}}{\alpha^2}\, z\right|),$$

whose asymptotic behavior for $z >> 1$ is

$$\frac{1}{\sqrt{2\pi}}\, \frac{1}{(1+\alpha^2)^{1/4}}\, \frac{1}{\sqrt{z}}\, e^{-\lambda z}$$

(K_0 is the modified Bessel function of the 2nd kind of order 0).

In our case,

$$\lambda = \frac{\sqrt{1+\alpha^2} - 1}{\alpha^2} \approx 0.25$$

and this p.d.f. decreases for large z much slower than a χ^2 with 3 degrees of freedom which behaves as

$$\sqrt{\chi^2_{(3)}}\ \ e^{-\chi^2_{(3)}/2}$$

For large values of T, and in our case where $N_{OFF} \approx N_{ON}$, we take the law of T to be that of z.

Finally, the "number of standard deviations" n is given by :

$$\frac{1}{\sqrt{2\pi}} \int_n^\infty du\, e^{-u^2/2} = \frac{1}{\sqrt{\pi k}} \frac{1}{(1+\alpha^2)^{1/4}} \int_{\sqrt{2\lambda \hat{T}}}^\infty du\, e^{-u^2/2}$$

where $\hat{T}$ is the value of T obtained with the sample being analyzed.

References

[1] 1.a G. Vacanti et al. Astro-Ph. J., 377 (Aug. 1991) 467

1.b C.W. Akerlof et al. N. Ph. B, 14A, Proc. suppl.(1990) 237

1.c P. Goret et al. (ASGAT exp.) To be published in A & A

[2] DELSIM reference manual: DELPHI 87-97:PROG-100

P. Baillon et al.: Description of the RICH simulation; DELPHI 87-103/PROG-102

[3] P. Schune Thesis, Un. Paris-sud , Mai 1990

[4] T. Socroun. Thesis, UN. Paris VII,June 1991,Int. Rep. LPNHEP 91-02

[5] O. Klein. Int. Rep. ; LPNHE Paris 6-7/1988

[6] O.C. De Jager et al. Astroph. J. 396 (1992) 161

[7] From 1] and

7.a D.E. Alexandreas et al. Astroph. J L.53 (1991) 226

7.b K.G.Gibbs et al. Proc. 22sd ICRC (1991) Vol.1, p 208

7.c M. Merck et al. Proc. 22sd ICRC (1991) Vol 1, p 261

7.d M. Amenomori et al. Phys. Rev. Lett. 69, 17 (1992) 2468

Figure captions

Fig.1: Lay-out of the 18 telescopes of the detector; also shown is the position of the tower supporting the calibration laser.

Fig 2: Trigger multiplicity distribution
Full line: Experimental distribution
Dotted line: M.C. generated distribution
The histograms are normalised to the same area.
The dotted curve is an exponential fit to the M.C. histogram.

Fig 3: Sum of the values of ADC's over all telescopes passing threshold, for each event giving a trigger.
Full line histogram: experimental events
Dotted line histogram: M.C. generated distribution
The histograms are normalised to the same area.

Fig. 4: Mean time residuals after fit of the cone for events with a fit probability ≥ 0.10
$\Delta T = < |$ T measured -T expected $|>$ in ns.

Fig 5: Average radial distributions of Cerenkov photon density for energies 1, 3, 10, 30 and 100 TeV, with their polynomial approximation superimposed. The average values have been obtained from statistics of 300 showers at 1 TeV to 12 showers at 100 TeV.

Fig 6: Distribution of "Hadronicity" for Monte-Carlo events (a) Gammas (b) Hadrons and for real events (c). The $\chi 2$ is reduced by dividing by the number of measurements.

Fig 7: Calculated error on energy for (a) Monte-Carlo hadrons (b) Real events

Fig 8: Subtracted bi-dimensional distribution in u_R, u_D variables, On-source - Off-source events. The Off-source is renormalized by the max. likelihood fit procedure. The bin size equals twice the value of the fitted width i.e. 2x2.26mr.

Fig.9: Distribution of the square of the angle between the Crab direction and the reconstructed cone axis: γ^2. The gray histogram is the On-source contribution. The hatched histogram is the off-source distribution renormalized by the max. likelihood fit.

Fig.10: A summary of the Crab flux measurements as a function of energy. Also shown are the points from ref. 1.a, 1.b, 7.a, 7.b, 7.c, 7.d..
The line $\Phi(>E) = 2\ 10^{-11}(E)^{-1.4}\ cm^{-2}s^{-1}$, is from ref: 1.a.

TABLE 1

	M. C. Gamma	M. C. Hadron	Real events
σ_{u_R} (C) (mr)	1.51	1.81	2.76
σ_{u_D} (C) (mr)	1.62	2.24	2.79
σ_{u_R} (D) (mr)	1.14 ± 0.01	1.60 ± 0.05	
σ_{u_D} (D) (mr)	1.27 ± 0.01	1.91 ± 0.05	
$\sigma_{x,y}$ (C) (m)	8	9	14
$\sigma_{x,y}$ (D) (m)	8 ± 1	13 ± 1	

TABLE 2

Events On / Off	6516 / 5647
Events in signal	282±54
σ signal	2.26±0.28
u_{Ro} (mr)	0.57±0.50
u_{Do} (mr)	0.24±0.36
S / B	0.58±0.10
Significance (N σ)	5.8

TABLE 3

E > (TeV)	3	5	7	9	11	13	15
Events On-source Off-source	4366 4606	4052 4260	3200 3301	2297 2312	1645 1595	1165 1159	856 785
Signal (Evts)	282±55	246±49	190±41	155±34	119±30	83±24	60±21
σ (mr)	2.44±0.29	2.37±0.30	2.16±0.28	1.88±0.25	1.88±0.26	1.93±0.21	1.94±0.44
u_{Ro} (mr)	-0.17±0.47	-0.08±0.58	0.02±0.46	-0.86±0.35	-1.05±0.39	-1.54±0.49	-1.90±0.85
u_{Do} (mr)	0.43±0.12	0.67±0.37	0.54±0.16	0.37±0.30	0.40±0.35	0.99±0.46	1.31±0.53
S/B	0.71± 0.10	0.69±0.10	0.81±0.20	1.29±0.30	1.31±0.30	1.19±0.20	1.12±0.30
Signif (n σ.)	6.5	6.1	5.7	6.3	5.5	4.5	3.6
Accept.	0.310	0.514	0.615	0.678	0.726	0.755	0.780
Flux (10^{-12}) ($cm^{-2}s^{-1}$)	6.8±1.3	3.7±0.7	2.3±0.5	1.70±0.37	1.22±0.31	0.82±0.24	0.57±0.20

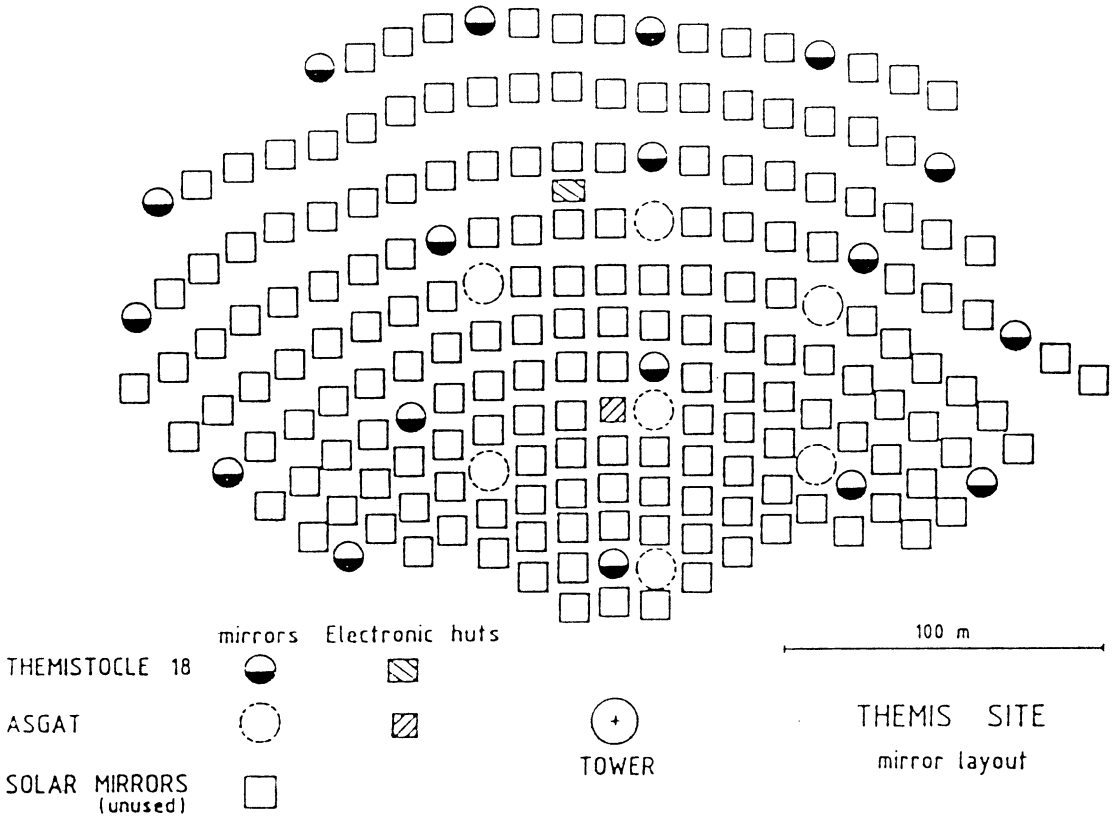
mirrors
Electronic huts
100 m
THEMISTOCLE 18
ASGAT
SOLAR MIRRORS
(unused)
TOWER
THEMIS SITE
mirror layout

Fig. 1

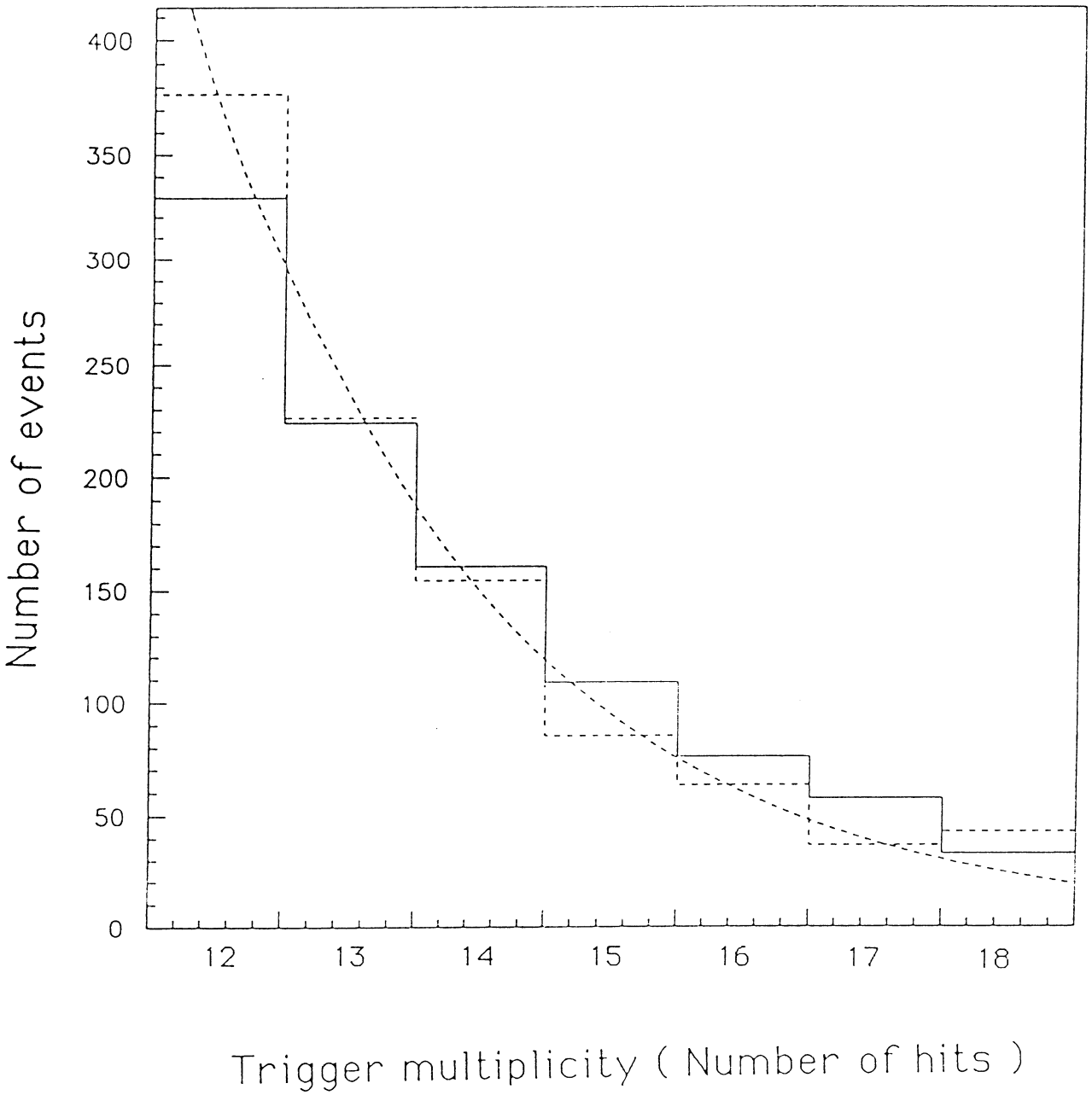
400
350
300
250
200
150
100
50
0
Number of events
12
13
14
15
16
17
18
Trigger multiplicity (Number of hits)

Fig. 2

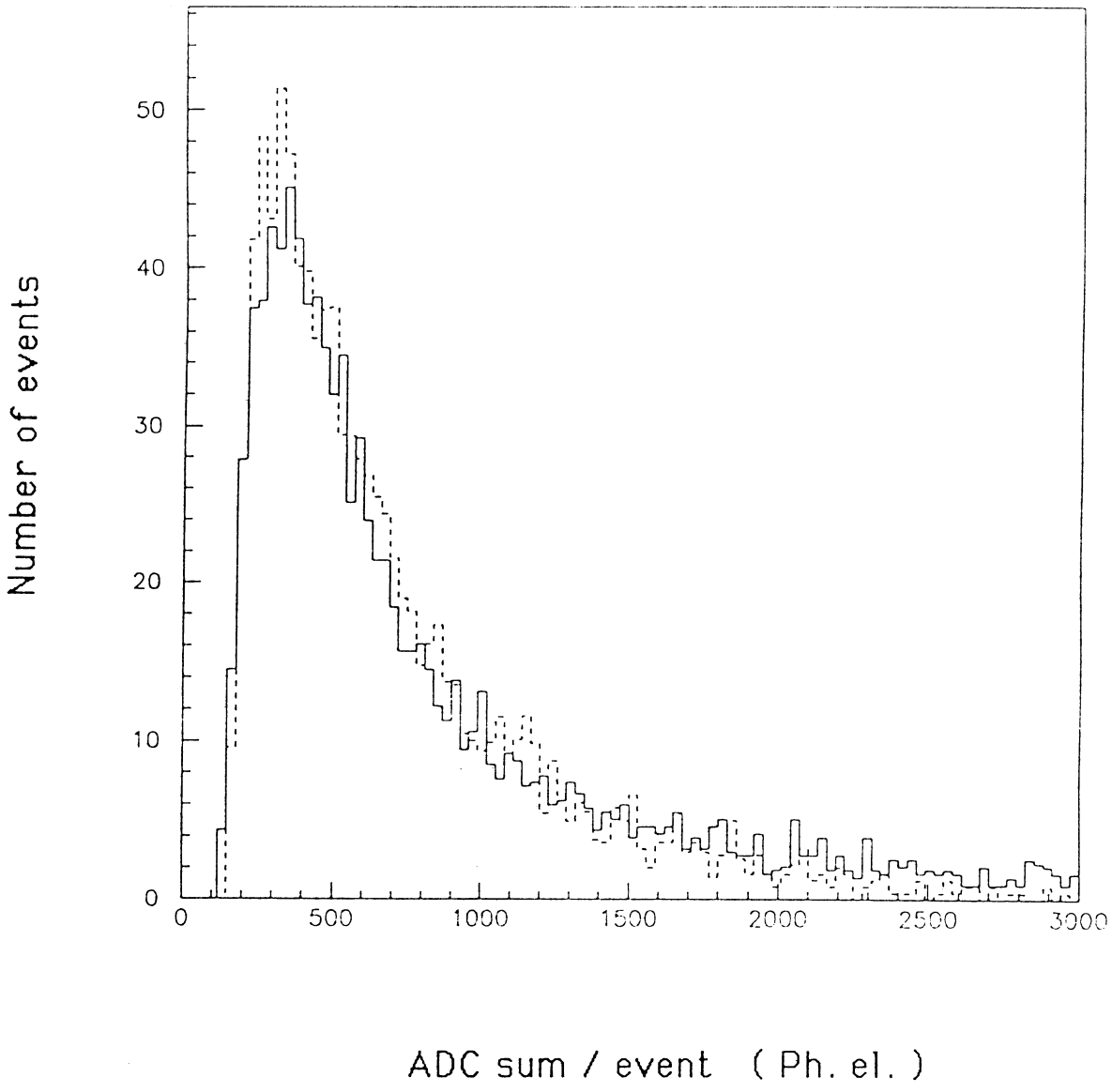
Number of events
50
40
30
20
10
0
0
500
1000
1500
2000
2500
3000
ADC sum / event (Ph. el.)

Fig. 3

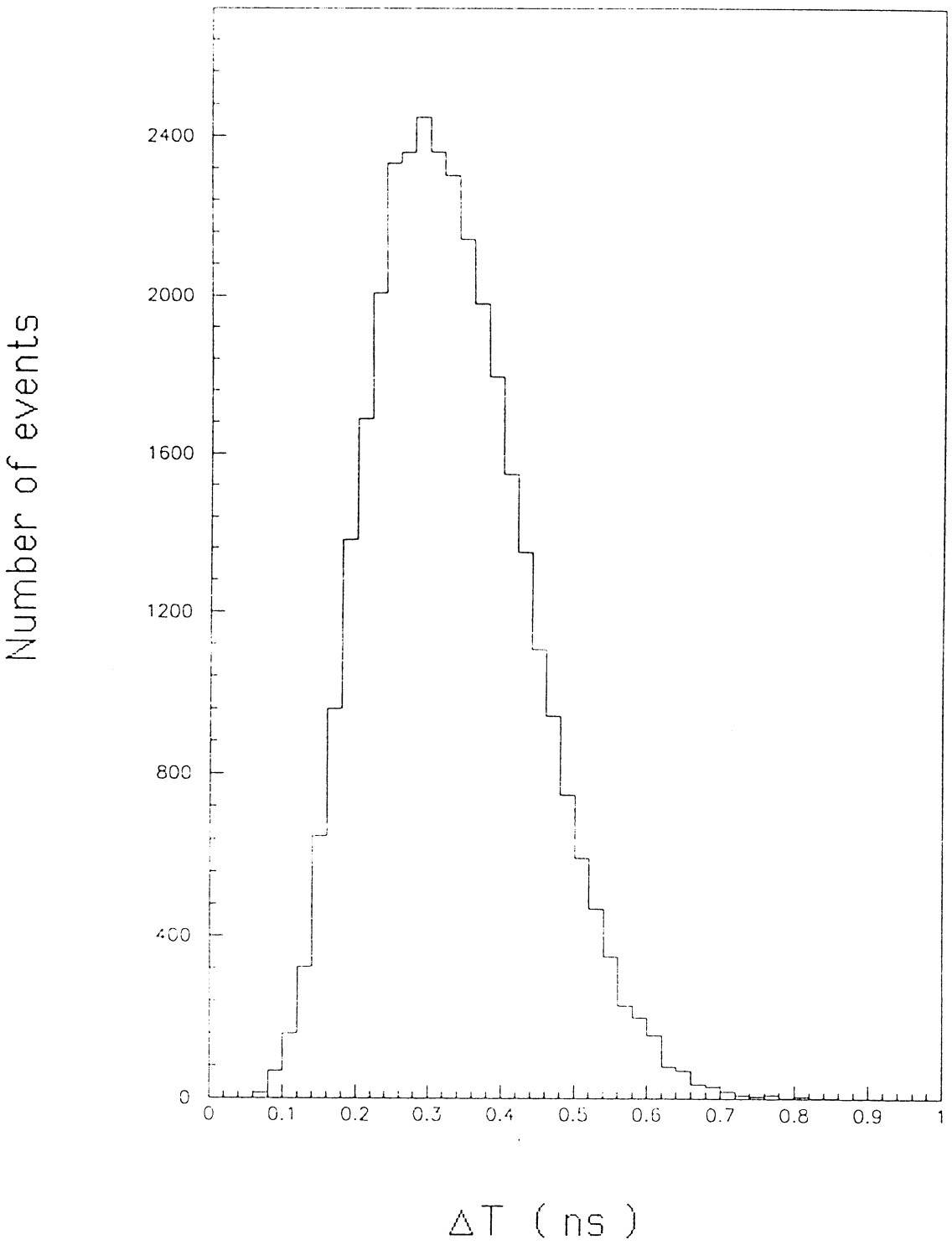
Number of events
2400
2000
1600
1200
800
400
0
0
0.1
0.2
0.3
0.4
0.5
0.6
0.7
0.8
0.9
1
ΔT (ns)

Fig. 4

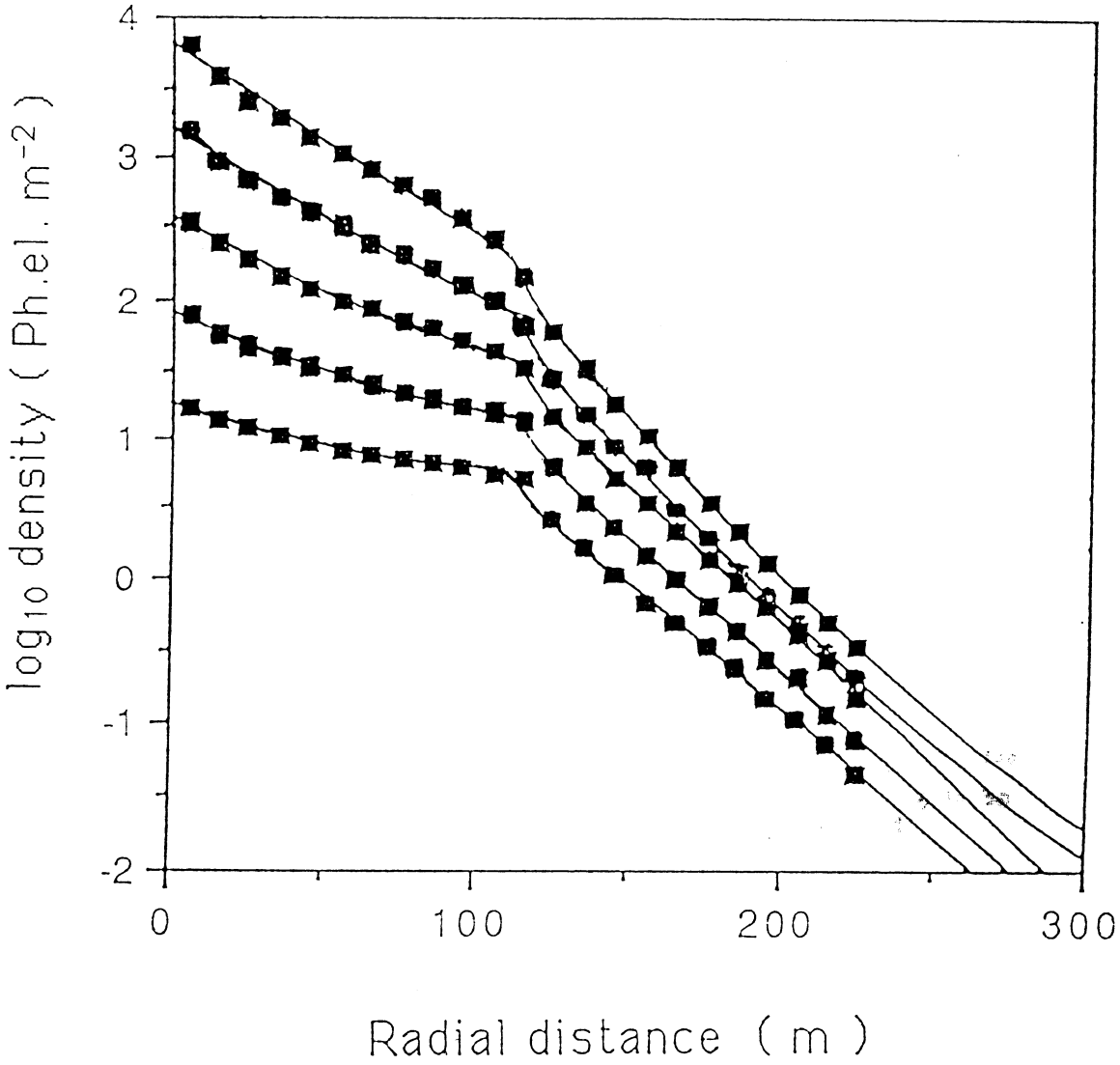
4
3
2
1
0
-1
-2
0
100
200
300
log10 density (Ph.el. m-2)
Radial distance (m)

Fig. 5

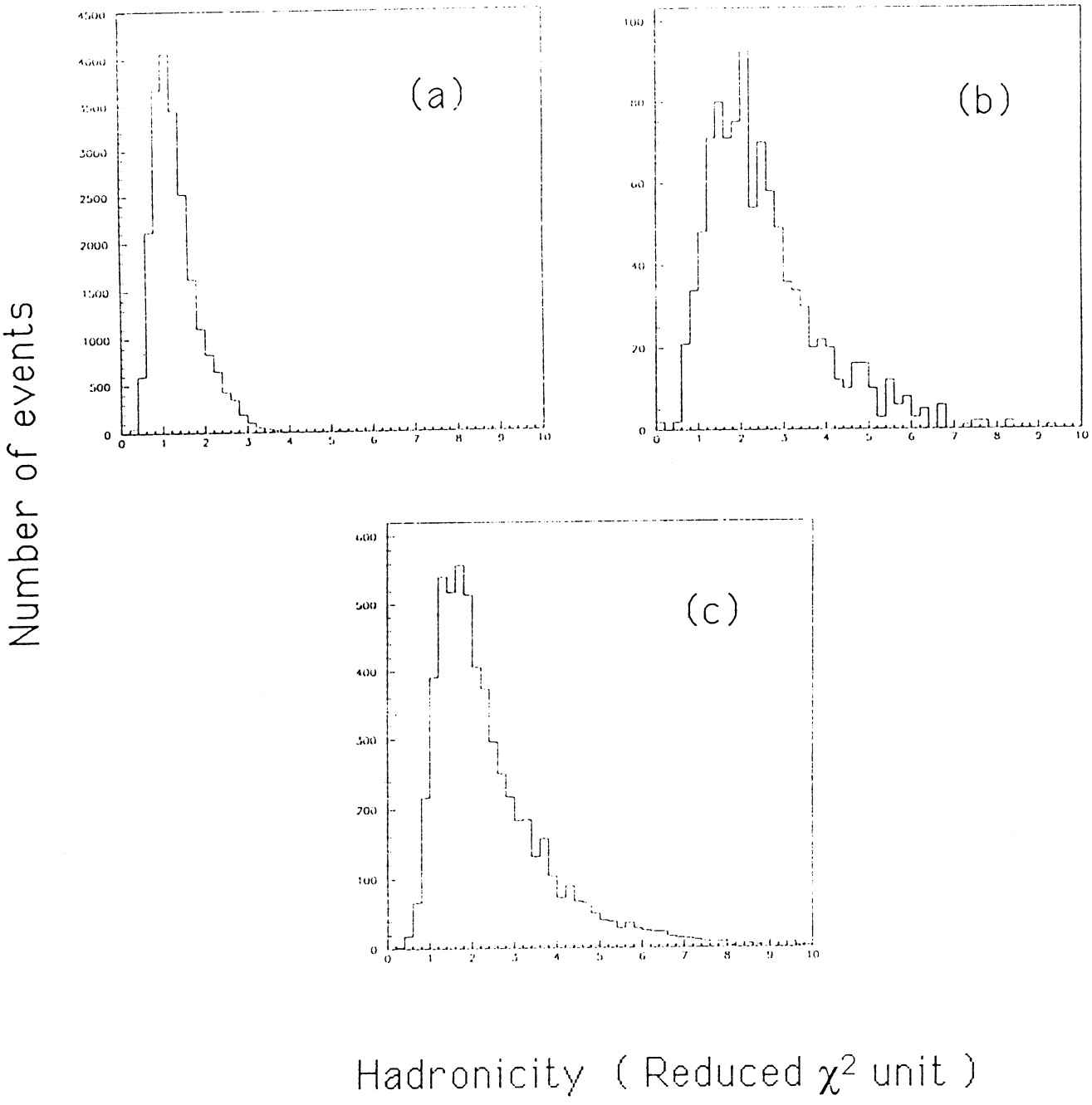

Fig. 6

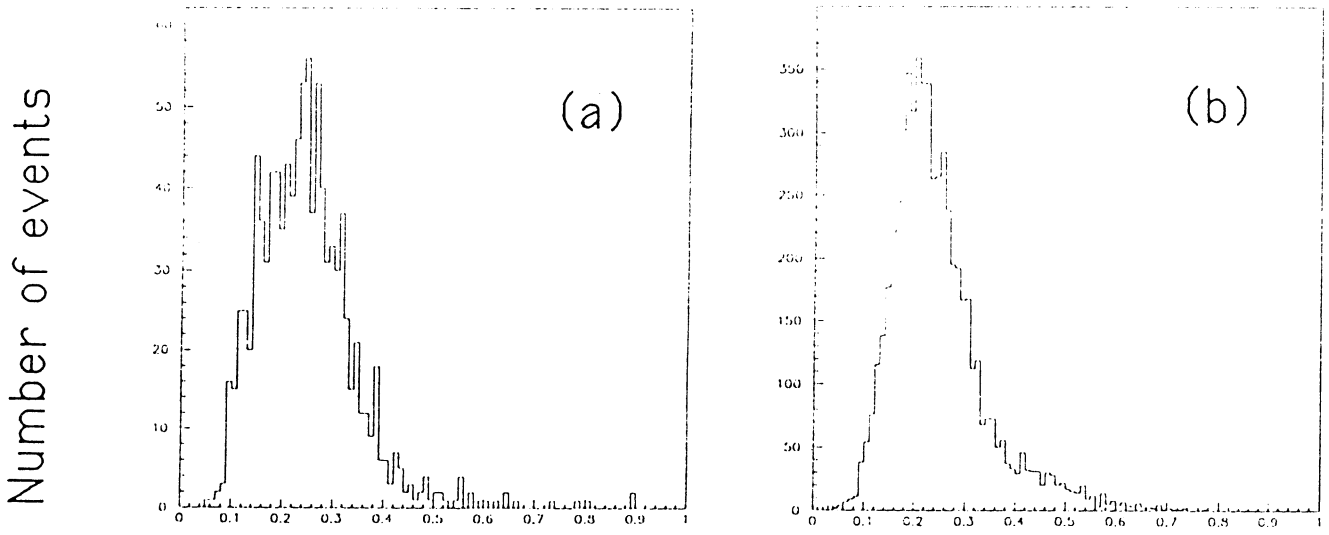

Fig. 7

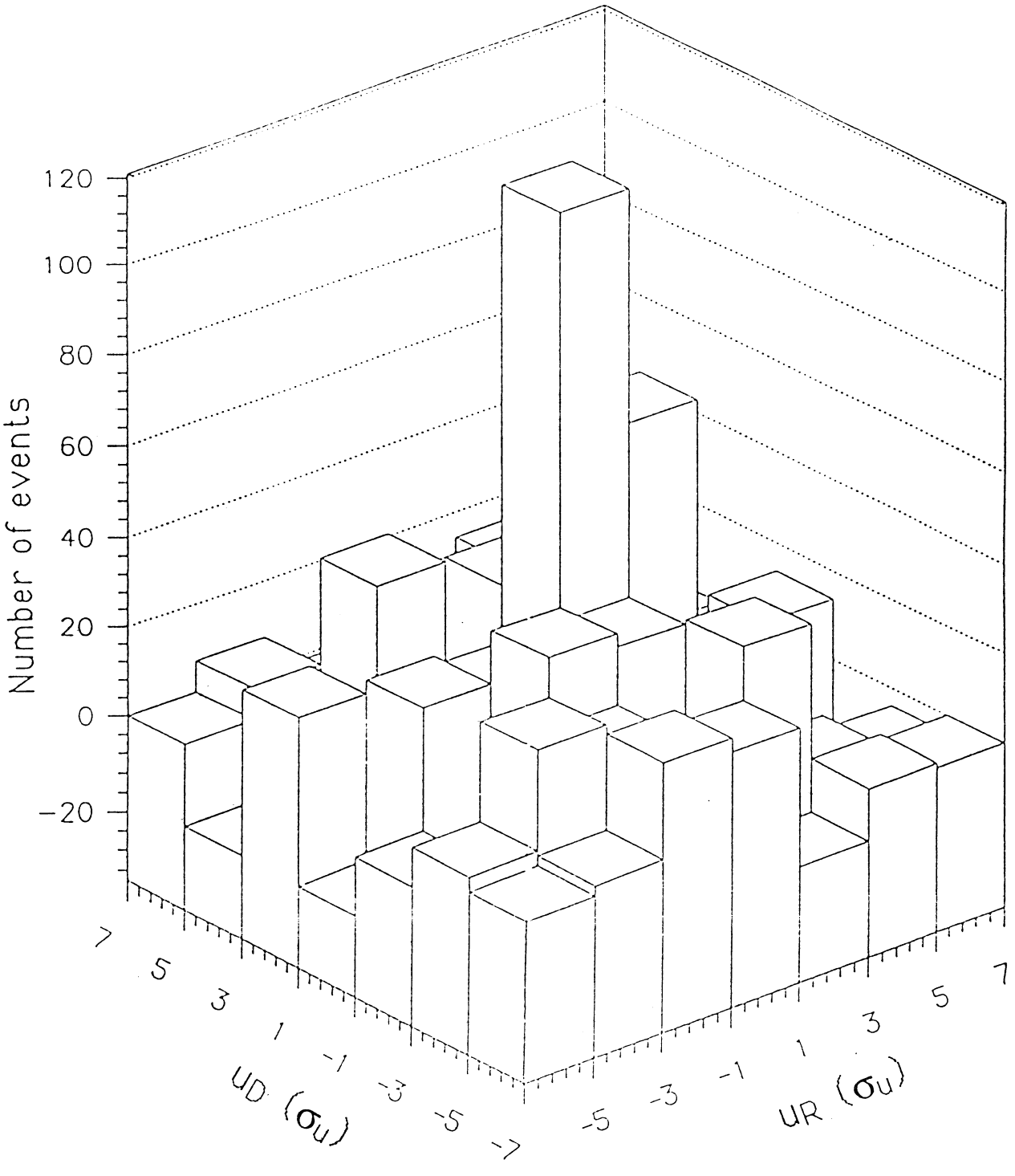
Number of events
120
100
80
60
40
20
0
-20
7
5
3
1
-1
-3
-5
-7
UD (σu)
-7
-5
-3
-1
1
3
5
7
UR (σu)

Fig. 8

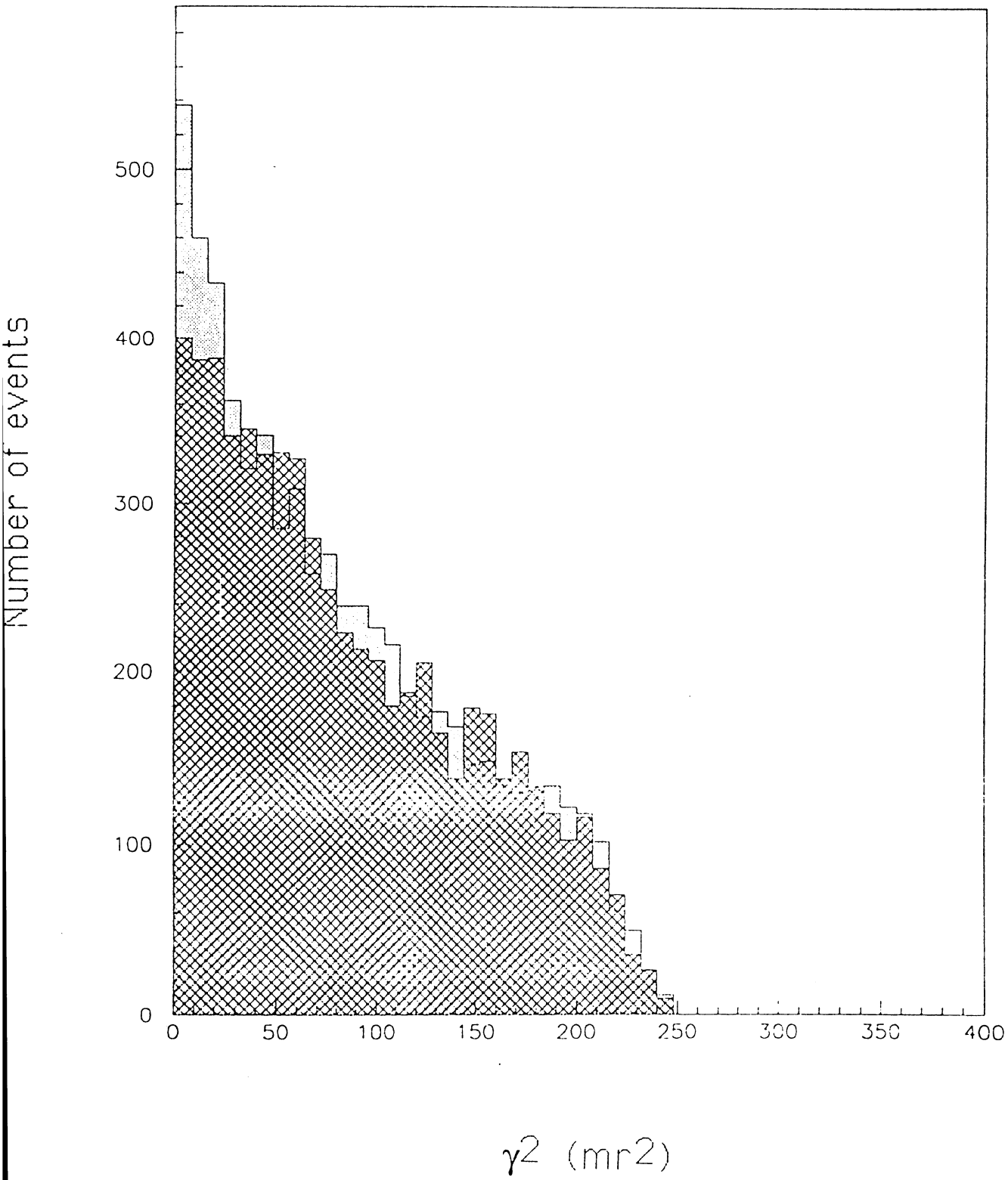
Number of events
500
400
300
200
100
0
0
50
100
150
200
250
300
350
400
γ2 (mr2)

Fig. 9

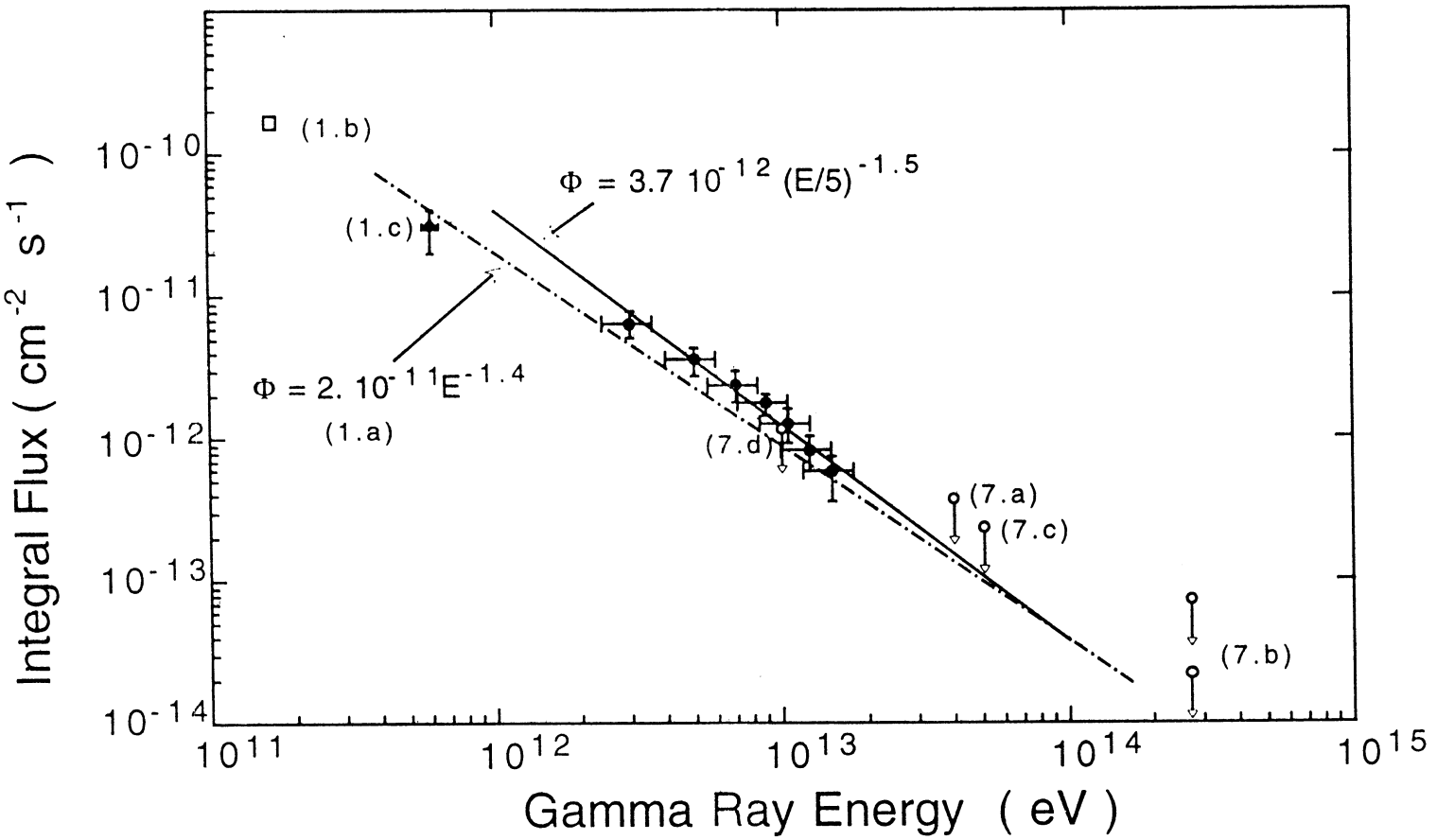
Integral Flux (cm^{-2} s^{-1})
10^{-10}
10^{-11}
10^{-12}
10^{-13}
10^{-14}
10^{11}
10^{12}
10^{13}
10^{14}
10^{15}
Gamma Ray Energy (eV)
(1.b)
(1.c)
$\Phi = 3.7\ 10^{-12}\ (E/5)^{-1.5}$
$\Phi = 2.\ 10^{-11} E^{-1.4}$
(1.a)
(7.d)
(7.a)
(7.c)
(7.b)

Fig. 10